Analysis and Programs for Assessment of Absorptive and Tilted Parallel Barriers

SIMON SLUTSKY AND HENRY L. BERTONI

An analysis and a computer program were prepared for use in connection with a FHWA test program. As part of this procedure, a model based on ray theory was developed for the prediction of highway traffic noise in the presence of tilted, absorptive barriers that are parallel to the roadway. The model was programmed for use on a personal computer or other DOS-compatible small computer. The program, called BarrierX, uses impedance of the barrier surface as input to compute the barrier reflection coefficients, which are therefore angle dependent. The program accounts for the modification of barrier reflection due to diffraction at discontinuities of the barrier surface impedance and at the discontinuity at the upper edges. Effects of atmospheric absorption, terrain absorption, and the pavement-wayside impedance discontinuity are taken into consideration. The highway and barriers are assumed to be straight and the wayside flat, but otherwise the program inputs permit considerable flexibility. Preliminary computations made with the program are in agreement with other recent studies, which conclude that parallel reflective barriers can severely reduce the anticipated single-barrier insertion loss and that absorptive wall treatment can be very beneficial. A result of considerable interest is that in roadway geometries of interest, relatively small angles of tilt can restore almost all of the single-barrier insertion loss.

This work was motivated by the need for a convenient method to predict the effect of tilt angle and absorptive treatment on the degradation of barrier insertion loss observed with parallel barriers. This degradation of barrier performance is a consequence of the reverberant reflection of vehicle-generated sound by the barrier surfaces.

The occurrence of such degradation is well documented in the literature. The recent work by Bowlby et al. (*1, 2*) contains comprehensive summaries of papers reporting predictions and measurements of degradation (*3, 4*). Hajek's predictions note the possibility of parallel barrier degradation of as much as 12 dB, depending on the barrier-source-receiver geometry (*4*). Such high degradation possibilities were also noted by Pejaver and Shadley (*5*). Bowlby et al. also called attention to Legillon's scale model measurements (*6*), in which the usefulness of tilting the barrier is noted and compared with absorptive treatment. The work of Bowlby and Cohn (*2, 7*) reflects the need for a modification of the STAMINA program (*8*) to include parallel barrier effects in a systematic way instead of by manipulation to create virtual highways. Bowlby and Cohn's computer program does not include the effect of barrier tilt; is based on a geometric acoustics approach so that it does not consider the fields reflected by the barrier discontinuities; and for the purpose of degradation, treats excess attenuation due to soft ground at the wayside as a constant. They report good comparison with data available to them.

The intent of this project is to account for the effect of barrier tilt and the diffraction phenomena that occur in the fields reflected by the barrier because of discontinuities of the reflective properties of the barrier, as well as to incorporate available improvements in the treatment of ground interaction at the wayside. Consideration of diffraction at reflective discontinuities demanded a departure from the use of the usual angle-averaged reflection coefficients in favor of the normal impedance to define the barrier surface materials. The reflection coefficient computed from the impedance is then angle dependent.

FHWA interest in dividing the barrier facing into several reflective zones (up to three) and the existence of a strong discontinuity at the top of the barrier made it necessary to treat diffractive effects at reflective discontinuities. Although a specific solution to this problem was not found in the literature, an approximate approach (strictly valid for only one reflection) was worked out on the basis of the Fresnel-Kirchhoff diffraction formula (*9, 10*). This impedance-based treatment of reflection was incorporated into a computer program called BarrierX.

As a stepping stone to BarrierX, a simpler program called Barrier was created first. This early program, like the one mentioned previously (*2*), was based on simple (geometric acoustic) ray theory, used angle averaged reflection coefficients as input, and did not include the effect of reflective discontinuities.

The treatment of excess attenuation caused by wayside absorption has been the subject of many works in the literature (*11–17*). The field is still very active, and there is much concern over the relative merits of the local soil reaction model (*11–15*) versus the extended reaction model (*16*). The latter assumes that the soil sustains wave propagation both vertically and horizontally, whereas the former assumes only a local surface interaction with no lateral interaction. The papers by Chien and Soroka (*14, 15*) have been widely referenced and used. The convenient expressions developed for computing and coding in their model are the basis of the subroutine module used in the current programs. Some versions of the extended reaction model, such as that developed by Attenborough et al. [(*16*); note also their corrections in that work to equations by Rasmussen (*17, 18*)], are not much more complicated to code. However, Rasmussen (*17, 18*) and Habault and

Polytechnic Institute of New York, 333 Jay St., Brooklyn, N.Y. 11201.

Corsain (*19*) have noted that for most soils and frequencies, there is not much difference in predictions made with the alternative models.

Another important area of investigation is the identification of the soil parameters that describe the acoustic character of the soil. A relationship between the characteristic impedance of an isotropic porous medium and the flow resistance is discussed by Morse (*20*). Delaney and Bazley (*21*) carried out extensive measurements and concluded that the normal impedance at the soil surface, as well as the soil/air sound speed ratio, could be predicted well by the air flow resistance. Other models are considered in the literature (*21*). Habault and Corsain (*19*) describe a general procedure for identifying the soil impedance by using a least squares curve fit to measurements from several (five or six) points on the ground. Nevertheless, because the Delaney-Bazley model is generally considered effective, it is used in the present programs. A convenient table of flow resistance for various soil types can be found in the work of Embleton (*24*).

Without exception, all theories that consider reflection of spherical or cylindrical waves from an impedance surface predict eventual attenuation of the field at the rate of 6 dB per doubling of distance in excess of the free field falloff rate. The distance at which that asymptotic decay rate is achieved depends primarily on the soil impedance, the frequency, and the angle of incidence of the specular ray. At smaller distances the theories may predict values of excess attenuation per doubling that may be either larger than or smaller than 1.5 dB/dd . For example, Attenborough (*23*) used several impedance models to compute the excess attenuation from a line of vehicles consisting of a mix of automobiles and trucks with typical emission spectra. His calculations included a variety of soil types for distances up to 72.8 m. Depending on the soil type and receiver height, Attenborough found values of excess attenuation per double distance that were sometimes much less than 1.5 and sometimes exceeded 3.0. His conclusion was that current schemes for predicting the attenuation of highway noise should be modified to include real impedance effects.

Rasmussen (*17, 25*) reported measured values of excess attenuation between pairs of points alongside a roadway that were as high as 8 dB/dd at some frequencies (notably 500 Hz). He also found that the influence of the pavement-wayside impedance discontinuity needed to be taken into account in some cases to get good agreement between measurements and predictions.

Atmospheric absorption is included in the current computer program by means of a table of attenuation in decibels per thousand feet versus humidity and frequency at a temperature of 68°F. This table is appended to the input template. Data are currently available for more general temperature conditions (*26, 27*) and can be incorporated into the program if desired. No account is taken here of wind gradients, temperature gradients, turbulence, and so on.

Input parameters used to define the roadway, the barriers, and the wayside, as well as the vehicular traffic volumes, types, and sound characteristics, are listed later in the paper in the section on the program treatment. Outputs are printed to the screen and echoed to the printer if desired. They consist of eight unweighted octave band levels from 63 to 8000 Hz, eight *A*-weight octave band levels, and the overall *A*-weighted SPL. This set of outputs is printed for each receiver.

ACOUSTIC PATH FIELDS

In this section, the various ray paths by which the fields radiated by a source can reach a receiver are summarized. If no barrier is present, these paths consist of the direct ray from the source to the receiver and the ray reflected from the ground. The presence of a single barrier complicates these paths by diffraction over the top of the barrier, and the presence of two barriers gives rise to additional ray paths because of the multiple reflections between the barriers.

Diffraction by a Single Barrier

The ray paths for a single tilted barrier between the source and receiver are shown in Figure 1. Rays reaching the top of the barrier can come directly from the source *S* or by reflection from the pavement. Subsequently, the diffracted rays from the barrier edge *E* reach the receiver *R* either directly or after reflection from the wayside, so that the total number of ray paths is four.

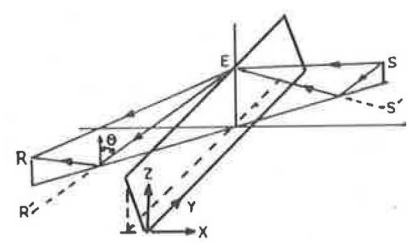

FIGURE 1 Diffracted path geometry.

Pavement Reflection

Reflection at the pavement may be treated by means of an image source at *S'*, whose strength is that of the actual source multiplied by the pavement reflection coefficient Γ. For an elevated barrier edge, the ray *SP* is never near glancing incidence, so the plane wave reflection coefficient may be used. Thus

$$\Gamma(\theta) = \frac{Z\cos(\theta) - 1}{Z\cos(\theta) + 1} \quad (1)$$

where Z is the pavement impedance normalized to that of the standard atmosphere and θ is the angle of incidence as measured from the normal to the pavement.

Barrier Diffraction

In treating diffraction at the barrier edge, the FHWA (Kurtze-Anderson) model has been adopted to facilitate comparison with other approaches and because of the speed of the resulting algorithm. This model introduces an insertion loss given in decibels by

$$\Delta = 0 \quad N \leq -0.1916$$

$$\Delta = 5.0 + 20 \log [NN/\tan (NN)] \quad -0.1916 \le N \le 0.0$$

$$\Delta = 5.0 + 20 \log [NN/\text{htan} (NN)] \quad 0.0 \le N \le 5.03$$

$$\Delta = 20.0 \quad 5.03 \le N \tag{2}$$

where

$$NN = \sqrt{2 \Pi |N|}$$

$$N = 2\delta/\lambda \tag{3}$$

Here, N is the Fresnel number, δ is the path length difference (which can be negative for uninterrupted paths), and λ is the acoustic wavelength. Δ is the insertion loss for the path due to diffraction.

Wayside Reflection: Homogeneous Ground

The problem of reflection of a point source by a plane surface has been investigated extensively since the beginning of this century. A long list of references and summary of results may be found in a review paper by Piercy et al. (*28*). Most of the discussion of this subject is concerned with the acoustic behavior of the ground, as well as with interpretation of the solutions. In particular, the question of local versus extended reaction of the ground has received much attention. K. B. Rasmussen discusses these matters in a useful series of papers and concludes that the local reaction model is quite similar to the extended model for typical values of surface impedance (*17, 18*).

The accepted model for including the effect of ground reflection, which is employed here, is to add the contributions of the direct path field reaching R from E in Figure 1 and the field that would reach the image receiver R' multiplied by the spherical wave reflection coefficient:

$$Q = \Gamma(\theta) + [1 - \Gamma(\theta)] * E(P_e) \tag{4}$$

where θ is the angle between the ray ER' and the normal to the ground, and $\Gamma(\theta)$ is as given in Equation 1. The function $E(P_e)$ is related to the complementary error function via

$$E(P_e) = 1 + i\sqrt{\pi} P_e \exp(-P_e^2) \operatorname{erfc}(-iP_e) \tag{5}$$

and the argument is

$$P_e = \sqrt{\pi i k r_2/2}\ (1/Z + \cos\theta) \tag{6}$$

where r_2 is ER', the slant distance from the point of diffraction at the barrier edge to the image receiver. In this program the wayside and pavement may have different elevations but are assumed to be parallel to each other, so that even when S and R are not opposite to each other across the barrier, all rays between S and R lie in the same (vertical) plane.

Delaney and Bazley (*21*) have developed a widely used semi-empirical relationship for the effective normalized acoustic impedance, Z, of porous soils that depends on the flow resistance, σ, of the soil and the frequency, f:

$$Z = 1 + 9.08\,(f_n)^{-0.75} + i\ 11.9\,(f_n)^{-0.73} \tag{7}$$

$$f_n = 1{,}000\, f/\sigma \tag{8}$$

This expression was found to give good agreement for a large number of soils and porous media. It is used as the basis for the current formulation of ground impedance.

Wayside Reflection: Impedance Discontinuity

Although the computer program is designed to deal with the effect of barriers, in some cases the barrier is of finite extent or is not present, so that propagation paths from some sources do not involve barrier diffraction. In these cases an impedance discontinuity exists between the pavement and the wayside.

In general, the effective reflection coefficient for this case will vary between the values determined by the two surface impedances, depending on what fraction of the Fresnel zone about the ray between the source S and image receiver R' intersects one or the other surface (see Figure 2). The Fresnel ellipsoid can be defined as the surface generated by the locus of points F (Figure 3) for which the direct path SR' and the broken path SFR' differ by a half wavelength. In addition to changing the effective reflection coefficient, the discontinuity in surface impedance will act as a line source for scattered rays propagating radially in all directions. One of these rays will reach the receiver R, contributing to the field there. Although various solutions to this problem exist, most take a long time to run on a microcomputer, especially at higher frequencies. In consequence, a semi-empirical expression developed by B. A. de Jong and described in detail by Rasmussen (*17*) has been used. The following expressions and discussion from de Jong's work are taken essentially verbatim from Rasmussen's description. This expression can be written as the normalized ratio of the combined field to the free field:

$$\frac{P}{P_f} = 1 + \frac{R_1}{R_2} \exp i\,k\,(R_2 - R_1) \begin{Bmatrix} Q_1 \\ Q_2 \end{Bmatrix}$$

$$+ (Q_2 - Q_1) \frac{\exp(i\,\pi/4)}{\sqrt{\pi}} \frac{R_1}{R_{34}}$$

$$\times \left[F_{341} + \begin{Bmatrix} + \\ - \end{Bmatrix} F_{342} \exp i\,k(R_2 - R_1) \right] \tag{9}$$

$$F_{341} = F\left[\, |k(R_{34} - R_1)| \,\right] \tag{10}$$

$$F_{342} = F\left[\, |k(R_{34} - R_2)| \,\right] \tag{11}$$

$$R_{34} = R_1 + R_1 \tag{12}$$

$$F(u) = \int_u^\infty \exp(i\,w^2)\,dw \tag{13}$$

$F(u)$ is the Fresnel integral, and the Q are defined by Equation 4. Q_1 and $+1$ are used when the specularly reflected ray path intersects Z1, and Q_2 and -1 are used when the ray intersects Z2 (Figure 3). The equation is valid only when Z1 represents the hard surface. The solution has the right form when Z1 = Z2 and when the specularly reflected ray strikes the discontinuity.

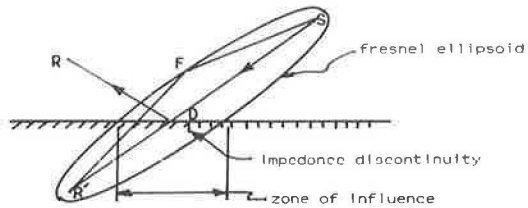

FIGURE 2 Fresnel ellipsoid for reflected path.

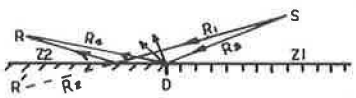

FIGURE 3 Diffraction from pavement-wayside discontinuity.

De Jong used the model in connection with model experiments and with outdoor measurements carried out with a loudspeaker source, with good agreement.

As noted above, there is some concern as to the justification of this approximation at large distances from the discontinuity. Experimental verification is not available for distances greater than 10 m. Until more confidence is established, the diffracted component will be set to zero when the discontinuity-to-receiver distance R_4 exceeds 100 ft (Figure 3).

COMBINED EFFECT OF PARALLEL BARRIERS

When two barriers are present, the ray fields reaching the barrier edge E closest to the receiver may undergo multiple reflections from the barriers and at most one reflection from the pavement. It has been found convenient to classify the rays according to the number of barrier reflections.

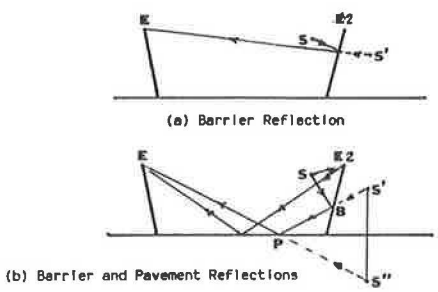

FIGURE 4 Diffracted paths with barrier reflection.

Single Reflection from a Barrier

The case of a single reflection is illustrated in Figure 4. If the ray is not reflected from the pavement, then the field reaching E can be constructed from an image source S', as indicated in Figure 4a, and the reflection coefficient of the barrier. To find the ray field reflected from the pavement, it is necessary to use S'' in Figure 4b, which is the image of S' in the pavement, and the pavement reflection coefficient given by Equation 1.

In addition to the reflected rays reaching E, a ray from S to $E2$ will excite diffracted fields propagating back toward E, either directly or via a pavement reflection. Moreover, if the surface of the reflecting barrier has different impedance in different horizontal bands, then diffracted rays will be excited at the impedance discontinuities. These complications are worsened because the Fresnel zone about the ray from S' to E may include the edge $E2$ or one of the impedance discontinuities (Figure 5). To overcome the difficulties introduced by these diffracted fields, an effective barrier reflection coefficient is used to account for the diffraction and accommodate barriers that have up to three horizontal bands with different surface impedance.

The effective reflection coefficient is obtained by using the physical acoustics approximation. The reflected field at the surface of the barrier is first written as the incident field multiplied by the local reflection coefficient. This field is then used in a Kirchhoff-Huygens integral to give the field at E. Division of this expression by the field for a perfect reflector gives the effective (pressure) reflection coefficient Γ_e. If the standard Fresnel approximations are made in the integral, the result is

$$\Gamma_e = \hat{\Gamma} + \frac{\exp(i\,\Pi/4)}{\sqrt{\Pi}} \operatorname{sgn}(\nu_1 - \hat{\nu})(\Gamma_2 - \Gamma_1)$$

$$\times F(|\nu_1 - \hat{\nu}|) + \operatorname{sgn}(\nu_2 - \hat{\nu})(\Gamma_3 - \Gamma_2)$$

$$\times F(|\nu_2 - \nu|) - \Gamma_3 F(|\nu_3 - \nu|) \qquad (14)$$

Here, Γ_1, Γ_2, and Γ_3 are the plane wave pressure reflection coefficients (Equation 1) of the lower, middle, and upper horizontal bands of the reflecting barrier. The term Γ is the reflection coefficient at the point of specular reflection at the barrier, and the functions $F(u)$ are defined by Equation 13. The quantities ν and ν_i (i = 1, 2, 3) are defined by

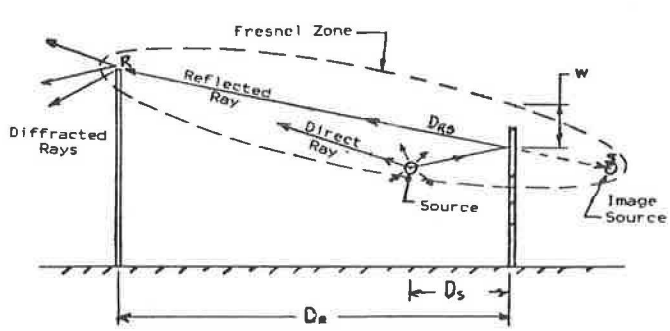

FIGURE 5 Reflection from multiple impedance surface.

$$\hat{v} = \hat{Z}\ \sqrt{k/2}\ \frac{(Dr + Ds)^2}{Drs\ \sqrt{Dr\ Ds\ Lrs}} \tag{15}$$

$$v_i = Z_i\sqrt{k/2}\ \frac{(Dr + Ds)^2}{Drs\ \sqrt{Dr\ Ds\ Lrs}} \tag{16}$$

$\hat{Z}$ is the height of the Fresnel point on the barrier, and Z_1, Z_2, and Z_3 are the heights of the discontinuities on the barrier. Dr, Ds, and Drs are the distances from the receiver to the reflecting barrier, from the source to the reflecting barrier, and from the receiver to the virtual source, respectively, as projected on the XZ plane (Figure 5). Lrs is the distance (in XYZ space) between the receiver and the virtual source. The half-width of the Fresnel ellipsoid at the barrier intersection is the reciprocal of the coefficient of Z in Equations 15 and 16, so that $(v_3 - v)$ is the nondimensional distance between the specular ray crossing and the upper edge discontinuity.

Expression 14 gives a continuous variation of the field as the specular point passes from one region of surface impedance to another. Because this expression includes both specularly reflected and diffracted fields, it can give values up to 17 percent higher, or as low as half of Γ_3. It is interesting that the reflection calculated by using Γ_e with the pavement-reflected ray in Figure 4b accounts for the diffracted ray originating at $E2$ that reaches E after being reflected by the pavement. Although Equation 14 is derived and is strictly valid only for a single barrier reflection, it is used subsequently for each barrier reflection of multiply reflected rays.

When no barrier is present on the side of the road nearest the receiver, reflections from the opposite barrier can still contribute to the field at the receiver. In this case the image source and appropriate reflection coefficients can be used to compute the reflected field without further introduction of diffraction.

Multiple Barrier Reflection for Zero Tilt

In Figure 6a, the element of multiple reflection for the simplified geometry of zero tilt is introduced. The barriers are numbered from the left ($B1$, $B2$, etc.). $B3$, $B5$, and $B7$ are virtual images of $B1$, and $B4$ and $B6$ are virtual images of $B2$. The zones between the barriers are similarly numbered, so that zone 1 contains real sources and all the subsequent zones contain the virtual sources of increasingly higher order. Virtual ray paths between the diffracting edge E of barrier 1 and all of the virtual sources are possible for this geometric configuration ($B1$ of equal or shorter height than $B2$ and its images). However, when $B1$ is taller than $B2$, as in Figure 6b, the higher-order paths fail to intersect $B2$ or its images, the reflections that define the ray do not occur, and then the ray itself cannot exist.

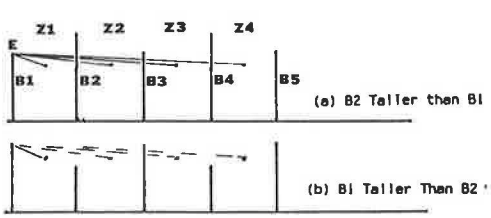

FIGURE 6 Multiple reflection for zero-tilt barrier.

Multiple Barrier Reflection with Tilt

The geometry of multiple reflection between parallel barriers is made more complicated by the presence of barrier tilt. Nevertheless, the construction of Figure 7 can completely rectify the apparently tangled real path (*29*). Because of the equality of angles of incidence and reflection for specular reflection, each ray segment and its virtual reflection are continued across each barrier as a straight line. Because this is true for virtual images of barriers as well as for the real barriers, the final virtual ray path can be displayed as a single straight line, independent of the number of reflections. Figure 8 shows an application of this construction to a more typical example of road geometry. It should be noted that if the ray crossing is above the top or below the bottom of the barrier, it cannot exist (as mentioned previously in the case of vertical barriers). Compatibility tests are therefore required for each ray contribution to locate the position of each assumed barrier crossing and to verify thereby the existence of the assumed reflections. It can be demonstrated that when either or both of the barriers are tilted, the compatibility test will always be violated after a finite number of barrier reflections (the number will depend on the height of the barriers, the width between barriers, and the tilt angles). This important result is the mechanism whereby the acoustically adverse effects of parallel barriers can be (almost) completely suppressed.

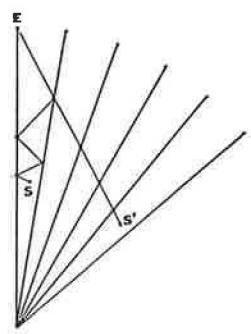

FIGURE 7 Multiple barrier reflection: wedge geometry.

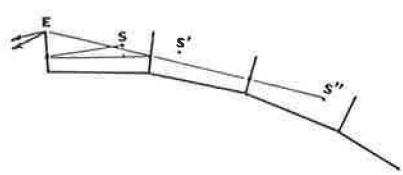

FIGURE 8 Multiple barrier reflection: tilted barriers.

In the present model, a limit of six zones is programmed for vertical barriers, and a limit of four zones is imposed for finite barrier tilt angles. Fewer zones can be specified by the user. It is assumed that four zones will be adequate for finite tilt because practical barrier configurations with tilt angles as small as 2 or 3 degrees show no acoustic contribution beyond the third zone. In general, the tilt angle required for suppression of multiple reflections is less as the ratio of barrier height to road width decreases. Some numerical aspects of this behavior are presented in the section on numerical results.

Multiple Barrier and Pavement Reflection

Another complication is introduced by reflection from the pavement. This effect is somewhat troublesome, as can be observed in Figure 9. This section of a prismatic cylinder shows the real pavement in Zone 1 and its images. The ray path between the virtual source in Zone 3 can reach the diffracting barrier edge E by a path that does not involve pavement reflection (as already considered above), or it can reflect from the pavement or one of its images, or it can do both. To locate the reflection point systematically, the image of the virtual source whereby the path can be rectified must be found. However, because three distinct reflective pavement surfaces exist for this case, three corresponding image locations must be tested for geometric compatibility. In Figure 9, ray SE satisfies the test. Not more than one pavement reflection is possible.

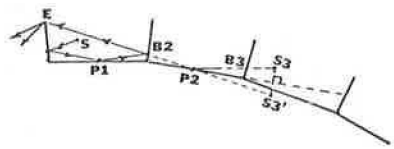

FIGURE 9 Tilted barriers with pavement reflection.

Finite Barrier Length Effects

None of the foregoing configurations takes account of the finite length of the barriers and their images. Figure 10 is a plan view of the base locations of the barrier pair, a single lane, and their images. Four principal cases can be identified:

- Case 1: Line of sight acoustic propagation between the source position and the receiver. This case is applicable only for sources in Zone 1.
- Case 2: Acoustic path with reflection off Barrier 2 but without encounter with Barrier 1. This case is applicable only for sources in Zone 2.
- Case 3: Acoustic path leading to diffraction at the top edge of Barrier 1 with subsequent paths to the receiver. The source can be real (Zone 1) or virtual (all other zones).
- Case 4: None of the above; the path is not viable.

PROGRAM TREATMENT

A critical step in this program is the separation of the speed, volume, and source characteristics from the barrier, highway, terrain, and atmospheric characteristics that could then be lumped into an insertion loss function H. The program is thus able to compute the total acoustic energy at a receiver as a product of the acoustic energy determined as if all the sources were in free space and a term that includes all modifications due to transmission loss from ground and pavement reflection, barrier reflection and diffraction, atmospheric absorption, and so on.

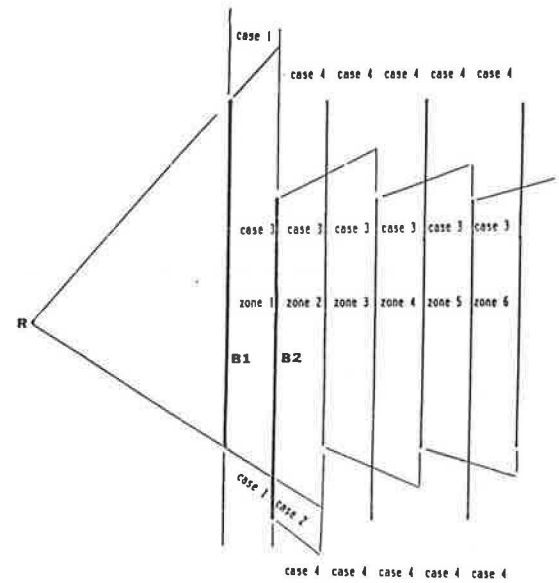

FIGURE 10 Case structure for finite barrier length.

Traffic Flow Integration

To sum the noise contributions of several streams of traffic, each with its own insertion losses due to various diffraction and absorption effect, a single source is considered, moving at constant speed along a representative path. That intensity can be expressed in the form

$$I_n = \frac{Q\,H_n}{4\,\Pi\,r_n^2} \tag{17}$$

where Q is the strength of the source, r_n is the unobstructed distance from source to receiver, and H_n is the correction factor, without which the expression would represent the free field intensity. Note that 10 log (H_n) is the insertion loss for the path. The source strength can be defined in terms of the free field intensity I_0 and the standard distance r_0 (50 ft):

$$I_0 = \frac{Q}{4\,\Pi\,r_0^2} \tag{18}$$

The total acoustic energy E accumulated at the receiver during a pass by is

$$E = \sum_n I_n\,\Delta t_n = \frac{1}{S}\sum_n I_n\,\Delta Y_n \tag{19}$$

where

S = source speed,
Y_n = Y coordinate of source, and
Δn = change in Y coordinate in time Δt_n.

Y_n can be expressed in terms of the X coordinate of the source and the angle θ_n between the X axis and the horizontal projection of the ray path (5), to obtain

$$E = \frac{I_0 r_0^2}{S X_{rs}} \sum H_n \Delta \theta_n \quad (20)$$

It should be noted that the $\Delta\theta$ increments add up to 180 degrees for the case of the infinitely long source path or to any other smaller value for the source path of finite length. Next, the equivalent intensity I_{eq} is obtained by dividing the pass-by energy E by the time between passes by $1/V$, where V is the traffic volume in vehicles per hour:

$$I_{eq} = \frac{I_0 r_0^2 V}{S X_{rs}} \sum H_n \Delta \theta_n \quad (21)$$

This expression must be generalized by incorporating the following extended definitions:

I_0 = I_0 (NV,NST,OCT),
V = VOL(NLAN,NV),
S = SPD(NLAN,NV) * 5280,
NV = vehicle type number (1 to NNV),
NST = source type number (1 to NNST),
NLAN = lane number (1 to NNLAN),
NZ = zone number (1 to NNZ),
OCT = octave band number (1 to 8), and
NR = receiver number (1 to NNR).

The source intensity is redefined in terms of the source strength:

$$I_0 \text{ (NV,NST,OCT)} = 10^{[LS(NST,NV,OCT)-55)/10]} * I_{REF} \quad (22)$$

where LS is the free field octave band sound pressure level at 50 ft. (The 55-dB term is arbitrary and is used to ease number handling. It is restored at final output.) The equivalent intensity corresponding to all zones, lanes, vehicle types, source types, and stations is found by summing to obtain a result EDEQ(OCT,NR), which depends only on frequency and receiver number. Note that no correction term is included for statistical variation of the source strength LS. The A-weighted equivalent intensity EDEQA(OCT,NR) is then obtained by using the AWT(OCT) corrections. EDEQ and EDEQA are printed out as the logarithms LEQ and LEQA. Finally, the LEQA are summed over the octave bands and printed out as the logarithm to obtain the A-weighted L_{eq}, LEQAWT(NR).

Program Input Parameters

The user can obtain an overview of the computer programs by examining the input parameters. The user has the option of specifying the following:

- Receiver number (NNR ≤ 20),
- Number of lanes (NNLAN ≤ 10),
- Number of source types (NNST ≤ 3/vehicle type),
- Number of vehicle types (NNV ≤ 5),
- Number of reflection zones (NNZ ≤ 6),
- Shoulder treatment (SHFLAG = 0 or 1; soft or hard),
- Lane dimensions (width of traffic lanes, median, shoulders, terrain strips, and Y-coordinates of pavement segment end points),
- Highway surface flow resistances (terrain, shoulders, median, and pavement),
- Barrier endpoints $X1$, $Y1$ to $X4$, $Y4$ (note that $X1 = X2$, $X3 = X4$),
- Barrier tilt angles (in degrees) and barrier panel widths (by barrier, panel),
- Barrier impedance or reflection coefficient (by barrier, panel, octave),
- Vehicle volume (per hour by lane and vehicle type),
- Vehicle speed (in mph, by lane and vehicle type),
- Source height (by vehicle type and source type),
- Source strength (free field at 50 ft, by vehicle type, source type, and octave band),
- Receiver parameters (coordinates X, Y, Z, ground elevation Z_g, and local ground flow resistance SIGG, for each receiver), and
- Atmospheric absorption (in dB/1,000 ft, each octave).

The parameters are entered by means of a special file that serves as an input template. Details and directions for using the template and the program will be found elsewhere (*30*).

ILLUSTRATIVE NUMERICAL RESULTS

It is interesting to examine the numerical behavior that is the result of the current work. Two kinds of behavior are examined below. The first is the influence of the ground interaction on numerical results without barrier complications, and the second is the behavior with barrier effects.

Figure 11 represents the excess attenuation (the field at the receiver in decibels minus the field that would exist there if the sound propagation were purely spherical, with no reflections, ground interaction or atmospheric attenuation, with sign changed) at various distances from a point source. The point source and the receiver are both at an elevation of 5 ft. The source is located over a hard pavement (flow resistance = 1.0 * 10^{10} N-sec/m^4), and the receiver is over soft soil (flow resistance = 3.0 * 10^5 N-sec/m^4). The strong ground effects are readily apparent and are characteristic of published results. Strong attenuation at grazing incidence can be seen. For example, at 500 Hz the excess attenuation per doubling of distance (dB/dd) varies from 4.4 in the interval 125–250 ft to 6.3 at 800–1600 ft. Note that these figures correspond to total values of 10.4 and 12.4 db/dd when they are combined with

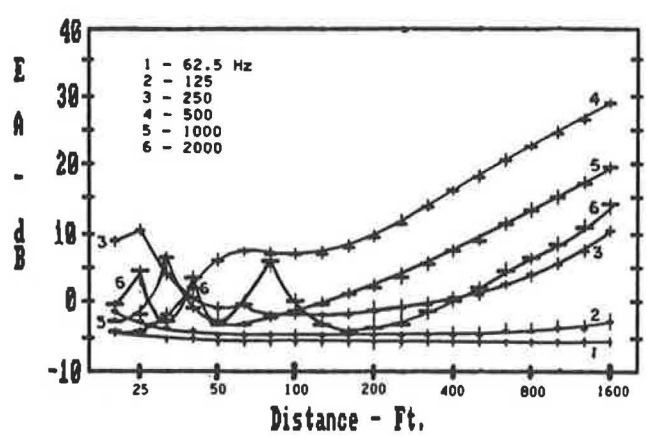

FIGURE 11 Excess attenuation for point source.

spherical spreading. The attenuation at 4 and 8 Khz (not plotted because the resulting figure would be confusing) is found to increase monotonically with distance, primarily because of atmospheric attenuation.

Figure 12 shows the situation for a line source and a receiver, both at elevation of 5 ft, with hard pavement and soft wayside. By comparison with Figure 11, it can be seen that the oscillations are damped by the effect of the line source averaging mechanism, but otherwise the curves have the same form. The excess attenuation per doubling of distance at 500 Hz again increases with distance, averaging 4.2 dB/dd between 125 and 250 ft, and 6.4 dB/dd between 800 and 1,600 ft, in marked contrast with the usual assumption of 1.5 dB/dd for soft ground in the FHWA and STAMINA models.

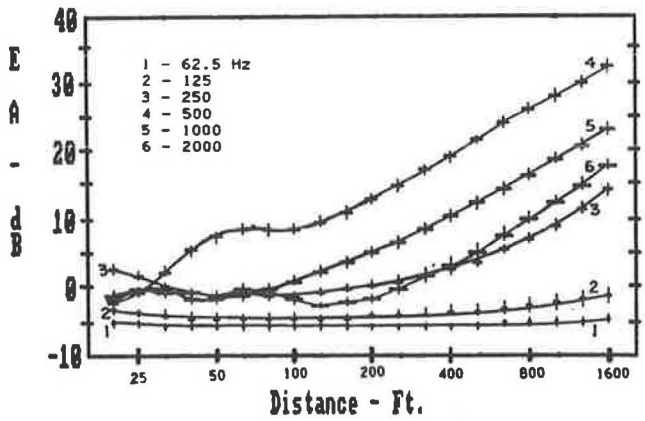

FIGURE 12 Excess attenuation for line source.

The next group of calculations is for the purpose of comparing the *A*-weighted SPL at a receiver caused by a line source in the presence of a single barrier with that due to several different coupled vertical barrier configurations. Figure 13 is for a 150-ft-wide roadway between 15-ft-wide barriers with a line source in the middle. The source heights range from 0.25 to 16 ft above the pavement. Although the tire spectrum that was used is applicable only at 0.25 ft, it was used for all elevations to simplify comparison. The receiver is located over hard terrain at a distance of 150 ft from the barrier base.

The solid curves were generated with program BarrierX (i.e., with Equation 14) for perfectly reflective barriers. The three curves in this group show the cumulative degradation effect of one, two, and five successive barrier reflections (corresponding to the effect of the five image roads) as compared to the case of the single barrier that has no barrier reflection paths. The degradation jumps most markedly as a result of the first barrier reflection, with reduced effect for subsequent reflections. The degradation from elevated sources is small. This is a result of the approach of the specular ray barrier crossing to the barrier edge, the approach of $\nu_3 - \hat{\nu}$ to zero in Equation 14, and the consequent decrease of Γ_e to half of Γ_3, with the corresponding reduction of the reflected intensity to 1/4 of what it would be from an infinite wall. Because multiply reflected rays from elevated sources are repeatedly attenuated in this way, they contribute less significantly. This attenuation mechanism also comes into play for some (but not all) of the multiple reflections from less elevated sources as the Fresnel half-width becomes large. This follows from Equation 15 or 16.

The dotted curves were generated by using Barrier for the same geometry and are based on geometric ray optics with local reflection coefficients (equal to unity for perfect reflection) at the specular reflection point. These curves change slowly with source elevation until the barrier height is exceeded, at which point the degradation drops abruptly. It will be noted that the neglect of (reflective) diffraction causes an overly pessimistic prediction of barrier performance.

Figure 14 presents a comparison of several barrier treatments with the single (no reflection) barrier case. The dotted curve labeled "1 - No Treatment" corresponds to the multiple (five) reflection result in Figure 13. The curve labeled "2 - Tilt 1°" displays a benefit of about 1 dB for sources below 5 ft elevation and a loss for elevated sources. A tilt angle of 3 degrees (Curve 3) displays improvement over the whole range of source heights, and a tilt angle of 5 degrees (Curve 4) displays (almost) total recovery for sources under 8 ft. Treatment of all panels with commercial fiberglass facing, with normalized impedance as presented in Table 1, resulted in Curve 5, "Absorption (All Panels)," which is everywhere within 1 dB of the single-barrier (zero-degradation) case.

One of the possible barrier treatments for investigation was that of absorptive treatment of a horizontal strip of the wall instead of the whole surface. Accordingly, in Figure 15 a comparison is made of the baseline (Curve 1, "No Treatment") and Curve 4, "Absorption (All)," both identical with those in

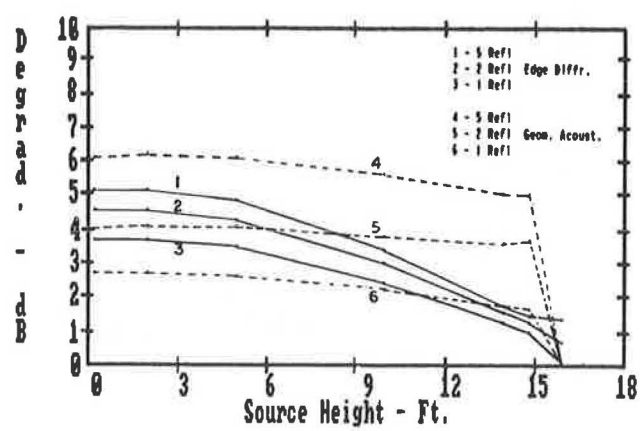

FIGURE 13 Barrier degradation: zone contributions.

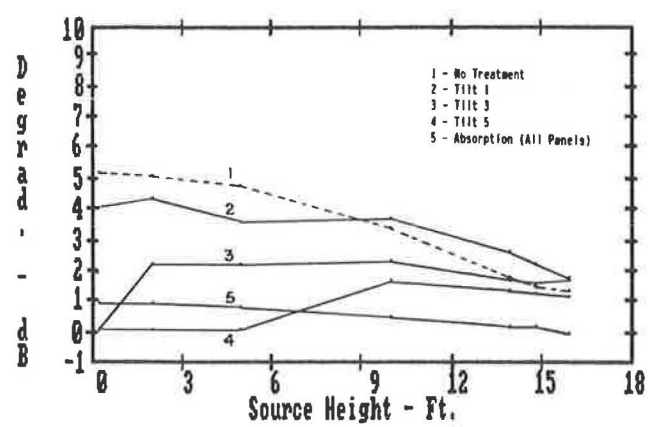

FIGURE 14 Comparison of tilt and absorption.

TABLE 1 NORMALIZED IMPEDANCE OF COMMERCIAL FIBERGLASS FACING

	Frequency							
	62.5	125	250	500	1000	2000	4000	8000
Real	3.51*	3.51	2.01	2.53	2.50	2.77	4.24	4.24*
Imag.	−4.85*	−4.85	−3.09	−0.69	−0.32	0.63	1.45	1.45*
Alpha	0.24	0.33	0.43	0.78	0.83	0.76	0.51	0.30

NOTE: Highway Barrier Test Material 3-in. 733, faced with 1.5 mi poly, hard backing.
*Estimated values.

Figure 14, with cases of partial barrier coverage. Curve 2, "Absorption (Top)," shows improvement over the "No Treatment" case for for elevated source positions, while Curve 3, "Absorption (Bottom)," shows improvement for lower sources. This behavior is physically reasonable but may be inadequate as a practical matter.

As noted, the results described are for a roadway with 150 ft between barriers. In Figure 16, it can be observed that degradation for a narrow road with 60 ft between barriers becomes more severe. Curve 2 is the "No Treatment" case, which compares unfavorably with the corresponding Curve 1 for the 150-ft roadway. A tilt of 5 degrees shows much less improvement than was obtained on the wider roadway and seems rather to have the same general behavior as the 1-degree tilt in Figure 14. A much larger tilt angle would be needed to recover effective barrier performance. Curve 4 is for a vertical wall on the side of the road nearer the receiver and a tilt of 20 degrees for the opposite wall. Full recovery can be observed except for extremely elevated sources, where the loss is less than 1 dB. Finally, a full absorptive treatment (Curve 5) is seen to restore practically full barrier performance.

Comparisons made with some of the Ullrich scale model insertion loss data reproduced by Bowlby et al. (*1*, Figure 3) for a depressed highway were not satisfactory for insertion loss but were good for degradation. The occurrence of Ullrich's barrier degradation of ~8 dB when the single barrier is replaced by the double wall is consistent with Curve 2 of Figure 16. The smaller width (52.5 ft) of the Ullrich model would result in slightly higher degradation than that for the 60-ft road shown in Figure 16. Curve 4 of Figure 16 (20-degree tilt) indicates almost no loss, whereas the scale model (25-degree tilt) shows

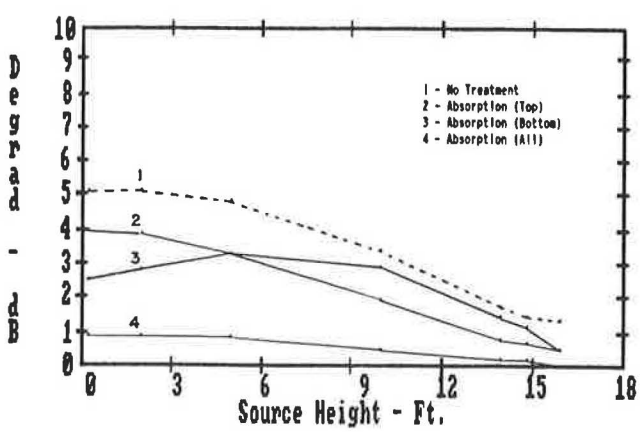

FIGURE 15 Partial absorptive treatment.

1–2-dB losses. Failure to get good agreement for insertion loss may be due to lack of detailed data on acoustic treatment of the (important) edge shoulder region of the depressed highway model.

Comparison with the scale model octave band insertion loss degradation measured by Hutchins (*1*, Table 7) shows that BarrierX loss predictions are generally higher by ~2–4 dB, but no clear trend is noticeable in the comparisons. Further study of these cases and of any other available experimental data would be desirable.

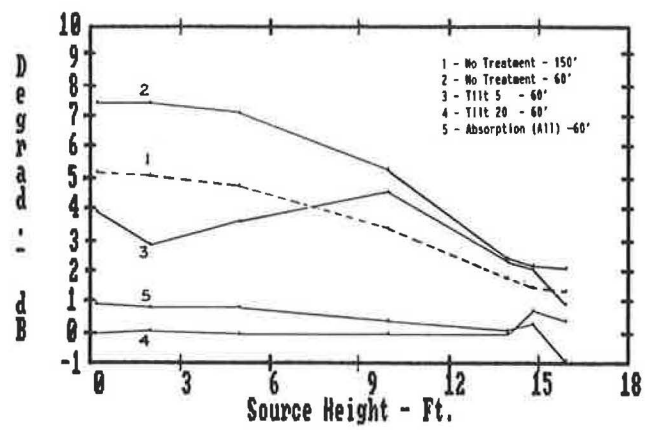

FIGURE 16 Effect of road width.

CONCLUSIONS AND RECOMMENDATIONS

A program has been constructed that can estimate the barrier insertion loss of parallel barriers that are tilted, or coated with acoustically absorbing materials, or both. The program takes into account some of the limitations of ray theory that are relevant when the acoustic wavelength is not small compared to the barrier height or to the width of the absorptive panels. This physical acoustics treatment is strictly valid only for the first barrier reflection and is only a reasonable approximation thereafter.

Predictions for degradation due to multiple reflections made with the physical acoustics program (BarrierX) are not as pessimistic as those made with the geometric acoustics program (Barrier). This decrease in degradation appears to be reasonable if the decreased effective reflectivity of a barrier when the Fresnel half-width becomes small compared to the distance from the specular reflection point to the barrier edge is considered.

Barrier tilt was found to be effective as a method of counteracting the degradation due to multiple reflection. Tilt

angles as small as 3 degrees were found to be effective for wide roadways (150 ft between barriers), and larger values (10 to 15 degrees) are needed for narrow roadways (60 ft between barriers).

Computations made to compare predictions from available scale model experiments reported in the literature show common trends. More experimental data are needed for validation of the program and for testing of confidence.

The program running time is 20 sec on a 6-MHz personal computer (PC) for the baseline case of one receiver, one zone, one lane, one vehicle type, and one source type. Total running time is then roughly proportional to the number of receivers, zones, and so on. Execution on a PC is convenient for exploring trends, but exercise of the program with repeated complex traffic configurations would probably be more convenient on a faster machine.

REFERENCES

1. W. Bowlby, L. F. Cohn, and R. A. Harris. A Review of Studies of Insertion Loss Degradation for Parallel Barriers. *Noise Control Engineering*, Vol. 28, No. 2, March–April 1987, pp. 40–54.
2. W. Bowlby and L. F. Cohn. A Model for Insertion Loss Degradation for Parallel Highway Noise Barriers. *Journal of the Acoustical Society of America*, Vol. 80, Sept. 1986, pp. 855–868.
3. J. J. Hajek. Effects of Parallel Highway Noise Barriers. In *Transportation Research Record 937*, TRB, National Research Council, Washington, D.C., 1983, pp. 45–52.
4. D. A. Hutchins, H. W. Jones, B. Paterson, and L. T. Russell. Studies of Parallel Barrier Performance by Acoustical Modeling. *Journal of the Acoustical Society of America*, Vol. 77, 1985, pp. 536–546.
5. D. R. Pejaver and J. R. Shadley. *A Study of Multiple Reflection in Walled Highways and Tunnels*. Rep. DOT-FH-11-8287. FHWA, U.S. Department of Transportation, 1976.
6. H. Legillon. Les Ecrans Absorbants en Bordure de Routes: Utilité et Caractérisation. *Bulletin de Liaison de la Laboratoire des Ponts et Chaussées*, Vol. 96, 1978, pp. 33–39.
7. W. Bowlby and L. F. Cohn. IMAGE-3: Computer-Aided Design for Parallel Highway Noise Barriers. In *Transportation Research Record 933*, TRB, National Research Council, Washington, D.C., 1983, pp. 52–62.
8. W. Bowlby, J. Higgins, and J. Reagan. *Noise Barrier Cost Reduction Procedure, STAMINA 2.0/OPTIMA: Users Manual*. Rep. FHWA-DP-58-1, April 1982.
9. S. Slutsky and H. L. Bertoni. *Parallel Noise Barrier Prediction Procedure Report 1: Description and Analysis of Tilted Absorptive Barriers*. U.S. Department of Transportation, June 1987.
10. B. B. Baker and E. T.Copson. *The Mathematical Theory of Huygens' Principle*. Oxford at the Clarendon Press, London, 1950, pp. 72–74.
11. A. Sommerfeld. Uber die Ausbreitung der Wellen in der Drahtlosen Telegraphie. *Annalen der Physik*, Vol. 28, 1909, p. 665 and Vol. 81, 1935, p. 1135.
12. H. Weyl. Ausbreitung elektromagnetischer Wellen über einem ebenen Leiter. *Annalen der Physik*, Vol. 62, 1920, p. 482.
13. B. Van Der Pol. *Physica*, Vol. 2, 1935, p. 843.
14. C. F. Chien and W. W. Soroka. Sound Propagation Along an Impedance Plane. *Journal of Sound and Vibration*, Vol. 43, 1975, pp. 9–20.
15. C. F. Chien and W. W. Soroka. A Note on the Calculation of Sound Propagation Along an Impedance Plane. *Journal of Sound and Vibration*, Vol. 69, 1980, pp. 340–343.
16. K. Attenborough, S. I. Hayek, and J. M. Lawther. Propagation Above A Porous Half-Space. *Journal of the Acoustical Society of America*, Vol. 68, 1980, pp. 1493–1501.
17. K. B. Rasmussen. *Sound Propagation Over Level Terrain*. Report 33. Acoustics Laboratory, Technical University of Denmark, 1982.
18. K. B. Rasmussen. Propagation of Road Traffic Noise Over Grass Covered Ground. *Journal of Sound and Vibration*, Vol. 78, 1981, pp. 247–255.
19. D. Habault and G. Corsain. Identification of Acoustical Properties of a Ground Surface. *Journal of Sound and Vibration*, Vol. 100, 1985, pp. 169–180.
20. P. M. Morse. *Vibration and Sound*. McGraw-Hill, New York, 1948, pp. 363–368.
21. M. E. Delaney and E. N. Bazley. Acoustical Properties of Fibrous Absorbent Materials. *Applied Acoustics*, Vol. 3, 1970, p. 1.
22. K. Attenborough. Acoustical Impedance Models for Outdoor Ground Surfaces. *Journal of Sound and Vibration*, Vol. 99, 1985, pp. 521–544.
23. K. Attenborough. Predicted Ground Effect For Highway Noise. *Journal of Sound and Vibration*, Vol. 81, 1982, pp. 413–424.
24. T. F. W. Embleton. Sound Propagation Outdoors. *Noise Control Engineering*, Vol. 18, No. 1, 1982, p. 33.
25. K. B. Rasmussen. Propagation of Road Traffic Noise Over Level Terrain. *Journal of Sound and Vibration*, Vol. 82, 1982, pp. 51–61.
26. *American National Standard Method for the Calculation of the Absorption of Sound by the Atmosphere*. Report ANSI S1.26-1978. Acoustical Society of America, New York, 1978.
27. J. E. Piercy and T. F. W. Embleton. *Handbook of Noise Control* (C. M. Harris, ed.), McGraw-Hill, New York, 1979, pp. 3–10.
28. J. E. Piercy, T. F. W. Embleton, and L. C. Sutherland. Review of Noise Propagation in the Atmosphere. *Journal of the Acoustical Society of America*, Vol. 61, 1977, pp. 1403–1418.
29. L. Cremer and H. A. Muller. *Principles and Applications of Room Acoustics* (T. J. Schultz, transl.), Vol 1, p. 40, Applied Science Publishers, 1982 pp. 105–116.
30. S. Slutsky. *Parallel Noise Barrier Prediction Procedure—Report 2: User's Manual*. U.S. Department of Transportation, June 1987.

Publication of this paper sponsored by Committee on Transportation-Related Noise and Vibration.